1 **Assessing the influence of water sampling strategy on the performance of tracer-**

2 **aided hydrological modeling in a mountainous basin on the Tibetan Plateau**

3 Yi Nan[1], Zhihua He[2], Fuqiang Tian[1], Zhongwang Wei[3], Lide Tian[4]

4 [1] Department of Hydraulic Engineering, State Key Laboratory of Hydroscience and Engineering,

5 Tsinghua University, Beijing, China

6 [2] Center for Hydrology, University of Saskatchewan, Saskatchewan, Canada

7 [3] Guangdong Province Key Laboratory for Climate Change and Natural Disaster Studies, School of

8 Atmospheric Sciences, Sun Yat-sen University, Guangzhou, Guangdong, China

9 [4] Institute of International Rivers and Eco-security, Yunnan University, Kunming, China

10 *Corresponding to*: Fuqiang Tian

11 Email: tianfq@tsinghua.edu.cn

Abstract

Tracer-aided hydrological models integrating water isotope module into the simulation of runoff generation are useful tools to reduce uncertainty of hydrological modeling in cold basins that are featured by complex runoff processes and multiple runoff components. However, there is little guidance on the strategy of field water sampling for isotope analysis to run tracer-aided hydrological models, which is especially important for large mountainous basins on the Tibetan Plateau (TP) where field water sampling work is highly costly. This study conducted a set of numerical experiments based on the THREW-T model to evaluate the reliance of the tracer-aided modeling performance on the availability of site measurements of water isotope in the Yarlung Tsangpo River (YTR) basin on the TP. Data conditions considered in the numerical experiments included the availability of glacier meltwater isotope measurement, quantity of site measurements of precipitation isotope, and the variable collecting strategies for stream water sample. Our results suggested that: (1) In high-mountain basins where glacier meltwater samples for isotope analysis are not available, estimating glacier meltwater isotope by an offset parameter from the precipitation isotope is a feasible way to force the tracer-aided hydrological model. Using a set of glacier meltwater $\delta^{18}O$ that were 2‰~9‰ lower than the mean precipitation $\delta^{18}O$ resulted in only small changes in the model performance and the quantifications of contributions of runoff components (CRCs, smaller than 5%) to streamflow in the YTR basin; (2) strategy of field sampling for site precipitation to correct the global gridded isotope product of isoGSM for model forcing should be carefully designed. Collecting precipitation samples at sites falling in the same altitude tends to be worse at representing the ground pattern of precipitation $\delta^{18}O$ over the basin than collecting precipitation samples from sites in a range of altitudes; (3) Collecting weekly stream water samples at multiple sites in the wet and warm seasons is the optimal strategy for calibrating and evaluating a tracer-aided hydrological model in the YTR basin. It is highly recommended to increase the number of stream water sampling sites rather than spending resource on extensive sampling of stream water at a sole site for multiple years. These results provide important implications for collecting site measurements of water isotope for running tracer-aided hydrological models to improve quantifications of CRCs in the high-mountain basins.

1. Introduction

43

44   Catchments located in mountainous regions generally provide important water resources
45 for downstream regions (Viviroli et al., 2003). As typical mountainous cryosphere, TP is the
46 source region for several large rivers in Asia, and has been called as 'water tower' because of
47 its importance for downstream livelihoods and agricultural irrigations (Schaner et al., 2012).
48 Dominant characteristic of mountainous catchments on TP is the multiphase of water sources
49 that generate runoff and the consequently complex hydrological processes, highlighting the
50 importance of accurately quantifying the contributions of runoff components (CRCs) to
51 streamflow for better understandings of the runoff dynamics under changing climate. This task
52 is difficult due to the complex hydrological processes being insufficiently represented by
53 typical hydrological models, leading to large uncertainty of hydrological simulations (He et al.,
54 2018). Due to the strong inter-compensation of runoff processes induced by different water
55 sources and runoff pathways (Duethmann et al., 2015), uncertainties of the modeled CRCs in
56 mountainous basins on the TP are rather high. Utilizing more datasets to evaluate the model
57 performance is a feasible way to constrain modeling uncertainty and improve quantifications
58 of CRCs in cold regions (Chen et al., 2017).

59   Tracer-aided hydrological models integrating environmental tracer (e.g., stable oxygen
60 isotope, ^{18}O) modules into runoff generation processes have proved helpful for parameter
61 calibration, model structure diagnosis and CRC quantification (Son and Sivapalan, 2007; Birkel
62 et al., 2011), and are increasingly adopted in cold catchments (e.g., Ala-aho et al., 2017; He et
63 al., 2019; Nan et al., 2021a). Recent researches indicated that estimates of precipitation $\delta^{18}O$
64 from outputs of isotopic general circulation models (iGCMs) perform well on forcing tracer-
65 aided models in large basins with a low cost of water sampling (Delavau et al., 2017; Nan et al.
66 2021b). Similarly to the tracer-based end-member mixing methods that utilize the different
67 tracer signatures of water sources to separate the hydrograph and quantify CRCs (Klaus and
68 McDonnell, 2013; He et al., 2020), the tracer-aided hydrological models used the differed
69 isotopic compositions of runoff components to constrain the water apportionments in runoff
70 generation. The isotopic compositions of runoff components strongly differ in high-mountain
71 basins resulting from the following two reasons: One is the significantly more depleted $\delta^{18}O$ of
72 meltwater compared to that of rain, due to the altitude and temperature effects, and the
73 fractionation effect during melting processes (Xi, 2014; Boral and Sen, 2020). Another is the
74 damping and lagging isotopic variability of subsurface runoff pathway, compared to that of
75 surface runoff, as a result of the catchment hydrological functions of storing, mixing and
76 transporting water (Bowen et al., 2019; Birkel and Soulsby, 2015; McGuire and McDonnell,
77 2006). Consequently, water isotope signatures bear good potentials to improve the
78 representations of internal hydrological processes in hydrological models, if observations of
79 water isotopes were involved in the model calibration and evaluation procedures (McGuire et

80   al., 2007; He et al., 2019).

81   Although a plenty of isotope-based works have been conducted in mountainous

82   catchments on the TP to improve understandings of local hydrological processes (e.g., Li et al.,

83   2020; Kong et al., 2019; Tan et al., 2021), bare of them provided guidance on data collection of

84   water isotope for hydrological applications in large mountainous areas. Some water sampling

85   works in large mountainous catchments were conducted in a single field campaign (e.g., Xia et

86   al., 2019; Dong et al., 2018), which is, although helpful to understand the generations of short-

87   term runoff events, not suitable for the calibration of tracer-aided models in a multi-year

88   simulation period (Knapp et al., 2019; Zhang et al., 2019). An exception is Stevenson et al.

89   (2021) who utilized a 7-year dataset of stream water $\delta^{18}O$ in a 3.2 km^2 catchment to analyze the

90   effects of stream water sampling strategies on the calibration of a tracer-aided hydrological

91   model. Challenges arise when transferring their findings to the application of tracer-aided

92   hydrological models in large high-mountain basins: First, it is questionable that whether

93   sampling stream water at one site can adequately represent the isotope signature of stream water

94   over the whole basin, considering the strong spatial variability of hydrological processes caused

95   by the heterogeneity in meteorological factors and land surface conditions in mountains (Wang

96   et al., 2021; Li et al., 2020). Second, the influences of data collection of precipitation isotope

97   on the performance of tracer-aided hydrological models remain unclear. Results of He et al.

98   (2019) indicated that monthly sampling of precipitation at two sites seems to be able to capture

99   the isotope variations in a 233 km^2 catchment. However, the requirement of isotope data

100   quantity to adequately capture the spatial pattern of precipitation isotope signature for forcing

101   tracer-aided models in large basins (~10^5 km^2) is poorly explored (Nan et al., 2021b). Third, in

102   glacierized mountainous catchments where streamflow was fed by additional water source of

103   glacier melt, the requirement of glacier meltwater samples for the forcing and evaluation of

104   tracer-aided hydrological models is also unclear. Consequently, better understandings of how

105   water sampling strategies influence the value of water isotope data for aiding hydrological

106   modeling, is highly helpful for guiding the establishment of monitoring systems of water

107   isotope in large mountainous regions. Considering the high costs of human and financial

108   resources of collecting water samples in TP area, it is important to take efficient strategies for

109   water sampling that balance the trade-off between field work burden and data adequacy well

110   (Sprenger et al., 2019).

111   Motivated by the mentioned backgrounds, we conducted detailed analysis on the tracer-

112   aided model performance in a large mountainous basin on the TP under different assumed

113   situations with respect to the collection strategy of site water isotope data, based on a numerical

114   experiment method. We adopted the tracer-aided hydrological model THREW-T developed by

115   Nan et al. (2021a), which was forced by the global gridded isotope outputs of iGCM being

116   corrected by measurements of precipitation $\delta^{18}O$, to achieve the research aim. Three specific

117   questions were addressed: (1) how does the estimated isotopic composition of glacier meltwater

118   influence the performance of tracer-aided hydrological modeling when no glacier meltwater

119   samples were available, (2) how does the collection strategy of site precipitation samples for

120   the correction of iGCM influence the model performance, and (3) how does the sampling

121   strategy of stream water influence the model calibration and evaluation?

122   **2. Materials and methodology**

123   **2.1 Study area**

124   The Yarlung Tsangpo River (YTR) basin, located in the southern TP (Fig. 1), extends in

125   the ranges of 27°N -32°N and 82°E -97°E, with an elevation extent of 2900-6900 m above sea

126   level (a.s.l.), which is one of the largest basins on the TP. The mean annual precipitation in the

127   YTR basin is around 470mm featured by a distinct wet season from June to September, due to

128   the dominance of the South Asian monsoon. Drainage area above the Nuxia hydrological station

129   at the basin outlet is approximately 2×10^5 km^2, and around 2% of which is covered by glacier.

130   The Karuxung River (KR) catchment is located in the upper regions of the YTR basin, and

131   was chosen as a supplementary experiment catchment, because of the long term field work of

132   water sampling in this catchment. The KR originates from the Lejin Jangsan peak of the Karola

133   mountain (7206m a.s.l.), and flows into the Yamdrok Lake (4550m a.s.l.), draining an area of

134   around 286 km^2. Streamflow in the KR catchment is strongly influenced by glaciers which

135   cover an area of 58 km^2.

136   **[Figure 1]**

137   **2.2 Hydro-meteorological and water isotope data**

138   Elevation of the YTR basin was derived from a digital elevation model (DEM) with a

139   spatial resolution of 30m from the Geospatial Data Cloud (https://www.gscloud.cn). Daily

140   meteorological inputs including precipitation, temperature and potential evapotranspiration

141   were collected from the 0.1°×0.1° China Meteorological Forcing Dataset (CMFD, Yang and

142   He, 2019). The second glacier inventory data set of China (Liu, 2012) and the Tibetan Plateau

143   Snow Cover Extent product (TPSCE, Chen et al., 2018) were used to denote the glacier and

144   snow coverages. Vegetation coverages were extracted from the MODIS satellite products of

145   eight-day leaf area index (LAI) dataset MOD15A2H (Myneni et al., 2015) and monthly

146   normalized difference vegetation index (NDVI) dataset MOD13A3 (Didan et al., 2015). Soil

147   types and properties in the tested basins were collected from the Harmonized World Soil

148   Database (HWSD, He, 2019). Observations of daily streamflow during 2000-2015 at the Nuxia,

149   and that during 2000-2010 at Yangcun and Nugesha stations were used for hydrological model

150   evaluation.

151   In the KR catchment, daily temperature and precipitation during 2006-2012 were collected

152   at the Langkazi meteorological station. Altitudinal distributions of temperature and

153   precipitation across the KR catchment were estimated based on the lapse rates reported in

154   Zhang et al. (2015). Daily streamflow during 2006-2012 was measured at the Wengguo

155   hydrological station.

156   Outputs of the scripps global spectral model with water isotopes incorporated (isoGSM,

157   Yoshimura et al., 2008) with the spatial and temporal resolutions of 1.875°×1.875° and 6h were

158   extracted to represent the spatio-temporal pattern of the precipitation isotope in the YTRbasin.

159   According to our previous evaluation of the isoGSM product, it overestimated precipitation

160    $\delta^{18}O$ in the YTR basin (Nan et al., 2021b). To correct bias in the isoGSM products, grab samples

161   of precipitation were collected in the wet season of 2005 at four stations along the main channel

162   of YTR, i.e., Nuxia (3691 m a.s.l.), Yangcun (4541m a.s.l.), Nugesha (4715m a.s.l.) and Lazi

163   (4889m a.s.l.). The precipitation water samples were collected as soon as possible after the

164   precipitation event in order to avoid the effect of evaporation. Stream water samples were

165   collected weekly during the same period from river at the four stations.

166   The isoGSM isotope products were corrected by Eqs. 1-3: First, the bias of isoGSM

167   product was assumed to be linearly related to altitude. Relation between the mean bias of

168   isoGSM products and altitude was estimated by a least square method using $\delta^{18}O$ measurements

169   of precipitation samples and gridded isoGSM estimates at the four sampling sites (Eqs. 1-2);

170   Second, on each grid of the isoGSM product, isoGSM estimate was corrected by a bias

171   estimated by the grid altitude in Eq. 3 based on the availability of $\delta^{18}O$ measurements from

172   precipitation site samples on the date.

173
$$B_i = \overline{\delta^{18}O_{i,M}} - \overline{\delta^{18}O_{i,G}} \tag{1}$$

174
$$B = a \cdot H + b \tag{2}$$

175
$$\delta^{18}O_{k,j,\text{Corr}} = \begin{cases} \delta^{18}O_{k,j,G} + B_k, & for\ date\ j\ with\ no\ data \\ \frac{\sum_{i=1}^{4} \delta^{18}O_{i,j,M}}{4} - \frac{\sum_{i=1}^{4} \overline{\delta^{18}O_{i,M}}}{4} + \overline{\delta^{18}O_{k,G}} + B_k & for\ date\ j\ with\ data \end{cases} \tag{3}$$

176   where, B_i is the bias of isoGSM at sites i. $\overline{\delta^{18}O_{i,M}}$ and $\overline{\delta^{18}O_{i,G}}$ are the weighted average of the

177   site measurement and isoGSM estimate over the sampling period at sites i, respectively. H is

178   the altitude of the sampling site. Parameters a and b are the linear regression coefficients, which

179   were estimated as -0.0046 and 14.96 by the least square method in this study. $\delta^{18}O_{k,j,\text{Corr}}$ is

180   the corrected isoGSM precipitation isotope, and $\delta^{18}O_{k,j,G}$ refers to the original isoGSM

181   isotope estimate at the hydrological model unit k on the date j.

182   Glacier meltwater $\delta^{18}O$ was assumed to be constantly lower than the weighted average of

183   precipitation $\delta^{18}O$ by an offset parameter (Δ_δ) during the study period (Eq. 4) because of the

184   unavailability of glacier meltwater samples, which is generally within the range of 2-9‰ in the

185 worldwide mountain regions (Rai et al., 2019; Wang et al., 2016; He et al., 2019; Ohlanders et
186 al., 2013; Jeelani et al., 2017) and is adopted as 5‰ from Boral and Sen (2020) in the YTR
187 basin.

188
$$\delta^{18}O_{k,\mathrm{GM}} = \overline{\delta^{18}O_{k,\mathrm{Corr}}} - \Delta_\delta \tag{4}$$

189 In the KR catchment, grab samples of precipitation and stream water were collected at the
190 Wengguo station in 2006-2007 and 2010-2012 for isotope analysis. The spatial distribution of
191 precipitation $\delta^{18}O$ was estimated based on an altitudinal lapse of -0.34‰/100 as reported in Liu
192 et al. (2007). Glacier meltwater $\delta^{18}O$ was assumed to be constantly as -18.9‰ during the study
193 period (similarly to Gao et al. 2009). Details of precipitation and stream water samples in the
194 YTR and KR catchments were summarized in Table 1.

195 **[Table 1]**

196 **2.3 Tracer-aided hydrological model**

197 A distributed tracer-aided hydrological model, THREW-T (Tsinghua Representative
198 Elementary Watershed - Tracer-aided version) model developed by Tian et al. (2006) and Nan
199 et al. (2021a) was adopted for streamflow and isotope simulations. This model uses the
200 representative elementary watershed (REW) method for spatial discretization of catchment
201 (Reggiani et al., 1999). The study catchment is first divided into REWs based on DEM, and
202 each REW is further divided into two vertical layers (surface and subsurface layers), including
203 eight hydrological subzones based on the land cover and soil properties. In total, 63 and 41
204 REWs were extracted for the YTR basin and KR catchment, respectively (Tian et al., 2020;
205 Nan et al., 2021a, 2021b). Areal averages of the gridded estimates of meteorological variables,
206 vegetation cover and soil property were calculated in each REW to drive the model. A module
207 representing glacier melting and snowpack evolution was incorporated into the model for
208 application in cold regions (He et al., 2015; Xu et al., 2019; Tian et al., 2020). The tracer-aided
209 module was developed by Nan et al. (2021a), which simulated the isotope mixing and
210 fractionation processes based on complete mixing assumption and Rayleigh fractionation
211 method (similarly to He et al. 2019; Hindshaw et al., 2011; Wolfe et al., 2007). Forced by the
212 inputs of precipitation and glacier meltwater isotopic compositions, the model simulates the
213 isotope evolution in all the water sources in the watershed, including stream water, soil water
214 and snowpack. The iGCM isotope products properly corrected by $\delta^{18}O$ measurements of
215 precipitation samples have proved feasible to force the THREW-T model in large catchments
216 like YTR on the TP (Nan et al., 2021b).

217 The THREW-T model quantified the contributions of runoff components (CRC) to
218 streamflow based on two definitions of runoff components as reviewed in He et al. (2021). The
219 first definition is based on the individual water sources in the total water input triggering runoff

220 processes, including rainfall, snowmelt and glacier melt. The second definition is based on

221 pathways of runoff-generation processes, resulting in surface and subsurface runoff (baseflow).

222 More details of the model description and setup are given in Tian et al. (2006) and Nan et al.

223 (2021a).

224   Physical basis and value ranges of the calibrated parameters in the THREW-T model were

225 described in Table 2. Two kinds of calibration approaches were conducted: (1) a bi-objective

226 calibration using discharge and SCA, and (2) a tri-objective calibration using discharge, SCA

227 and stream water $\delta^{18}O$. Metrics used to evaluate the model performance are listed in Eqs. 5-8.

228 The Nash-Sutcliffe efficiency coefficient (NSE) was used to optimize the simulation of

229 discharge and isotope, whereas the root-mean-square error (RMSE) was used for the evaluation

230 of SCA simulation. The Logarithmic Nash-Sutcliffe efficiency coefficient (lnNSE) was used

231 additionally for discharge calibration to assess the simulation of baseflow. The model

232 parameters were calibrated by streamflow and SCA observations during 2001-2010 (at Nuxia

233 station) and 2006-2012 in the YTR and KR basins, respectively. The model performance in

234 YTR basin was evaluated by the Nuxia streamflow and SCA observations during 2011-2015,

235 and the streamflow observations at Yangcun and Nugesha stations during 2001-2010.

236
$$NSE_{dis} = 1 - \frac{\sum_{i=1}^{n}(Q_{o,i}-Q_{s,i})^2}{\sum_{i=1}^{n}(Q_{o,i}-\overline{Q_o})^2} \tag{5}$$

237
$$NSE_{lndis} = 1 - \frac{\sum_{i=1}^{n}(\ln Q_{o,i}-\ln Q_{s,i})^2}{\sum_{i=1}^{n}(\ln Q_{o,i}-\overline{\ln Q_o})^2} \tag{6}$$

238
$$RMSE_{SCA} = \sqrt{\frac{\sum_{i=1}^{n}(SCA_{o,i}-SCA_{s,i})^2}{n}} \tag{7}$$

239
$$NSE_{iso} = 1 - \frac{\sum_{i=1}^{n}(\delta^{18}O_{o,i}-\delta^{18}O_{s,i})^2}{\sum_{i=1}^{n}(\delta^{18}O_{o,i}-\overline{\delta^{18}O_o})^2} \tag{8}$$

240 where, n is the total number of observations. Subscripts of "o" and "s" refer to observed and

241 simulated variables, respectively.

242   An automatic algorithm Python Surrogate Optimization Toolbox (pySOT) developed by

243 Eriksson et al. (2017) was adopted for the multiple-objective optimization. The pySOT

244 algorithm used a surrogate model to guide the search for improved solutions, with the advantage

245 of needing few function evaluations to find a good solution. In each pySOT running, the

246 optimization procedure was stopped if a maximum number of allowed function evaluations was

247 reached, which was set as 3000 in this study. For the bi- and tri-objective calibrations,

248 $0.5 \cdot (NSE_{dis}+NSE_{lndis})$-$RMSE_{SCA}$ and $0.5 \cdot (NSE_{dis}+NSE_{lndis})$-$RMSE_{SCA}+NSE_{iso}$ were chosen as

249 the combined optimization objectives. For each scenario, the pySOT algorithm was repeated

250 100 times, and behavioral parameter sets were selected among the 100 final results according

251 to the performance metric thresholds, i.e., only the parameter sets producing metrics better than

252 certain threshold values were regarded as behavioral parameter sets. The threshold values of

253 evaluation metrics were used as $0.5 \cdot (NSE_{dis}+NSE_{lndis})>0.8$, $RMSE_{SCA}<0.08$ in the YTR basin;

254   and NSE_{dis}>0.7, $RMSE_{SCA}$<0.15 in the KR catchment.

255   **[Table 2]**

256   **2.4 Numerical experiments**

257   **[Table 3]**

258   *Experiment 1: influence of assumed glacier meltwater isotope*

259   The first experiment was designed to test the reliance of model performance on the

260   assumed glacier meltwater isotope, as glacier melt water samples are typically not available for

261   isotope analysis in high mountain basins on the TP. In this experiment, variable glacier melt

262   isotope signatures were used to force the model, assuming the glacier meltwater $\delta^{18}O$ is 1‰,

263   3‰, 7‰ and 9‰ (i.e., Δ_δ values in Table 3) lower than the long-term average $\delta^{18}O$ of

264   precipitation. A benchmark model running by the literature based Δ_δ value of 5‰ was used as

265   a baseline reference to assess the influence of the assumed glacier meltwater isotope on the

266   model performance.

267   *Experiment 2: influence of site measurement of precipitation isotope*

268   The second experiment was designed to test the reliance of the model performance on the

269   availability of measured site precipitation isotope that was used to correct the isoGSM product.

270   The benchmark model running was forced by corrected isoGSM based on measurements of

271   precipitation isotope from all the four sampling sites (Figure 1). Three scenarios regarding the

272   availability of measured precipitation isotope were designed as shown in Table 3. First, we

273   assumed that only precipitation isotope measured at the two downstream sites of Nuxia and

274   Yangcun are available for the correction of isoGSM (i.e., scenario P_2stationNY in Table 3).

275   Second, we assumed that precipitation isotope measurement at the most upstream site Lazi is

276   available in addition to the measurement at the downstream site Nuxia (i.e., scenario

277   P_2stationNL in Table 3). Third, we assumed that only precipitation isotope measurement at

278   the most downstream site Nuxia is available for the correction of isoGSM (i.e., scenario

279   P_1station in Table 3).

280   *Experiment 3: influence of stream water sampling strategy*

281   The third experiment was conducted to analyze the influence of stream water sampling

282   strategy on the model performance. Two types of stream water sampling strategies were

283   considered, i.e., a time series sampling strategy based on regular and continuous sampling work

284   at a certain point, and a spatially distributed sampling strategy based on one-time field

285   campaigns of sampling work. For the time series sampling strategy, 7 scenarios (scenarios begin

286   with "RT_YTR_" in Table 3) were designed to analyze the influences of the sampling frequency,

287   the duration of the sampling period, and the number of sampling sites. For the spatially

288 distributed sampling strategy, two scenarios (Figure 1b) were designed to represent typical field

289 campaign activities: colleting samples along the mainstream of the basin (RS_YTR_Main,

290 Table 3), and collecting water samples additionally from major tributaries (RS_YTR_Tributary,

291 Table 3). Considering the limited availability of stream water $\delta^{18}O$ measurement in the YTR

292 basin (only wet season in one year, Table 1), a supplementary experiment was designed to test

293 the influence of sampling period duration on the model performance using the relatively long

294 time-series isotope dataset in the small catchment KR (scenarios begin with "RT_KR_" in Table

295 3).

296   To evaluate the influence of isotope data availability on the model performance, we carried

297 out benchmark model simulations forced by full datasets of input isotope and stream water

298 isotope data in the YTR and KR catchments (Table 3). The benchmark model runs were

299 calibrated by a bi-objective calibration using SCA and streamflow observations, and a tri-

300 objective calibration using additional stream water isotope, respectively. It is noted that, in

301 experiments that were carried out in the YTR basin (i. e., scenarios start with "RT_YTR_" and

302 "RS_YTR_" in Table 3), assumed stream water $\delta^{18}O$ measurements were adopted from model

303 simulations driven by a benchmark parameter set, which was selected from the behavioral

304 parameters of the BM_YTR calibrated by tri-objective approach, because the assumed data

305 availability was beyond the actual measurement dataset. The assumed stream water $\delta^{18}O$

306 measurements thus were not used to evaluate the model performance in simulating stream water

307 isotope. Instead, the influence of the availability of stream water $\delta^{18}O$ measurement on the

308 tracer-aided model were evaluated by comparing the estimated CRCs and corresponding

309 uncertainties with the assumed true values that were derived from the tri-objective calibrated

310 benchmark running. Mean absolute error (MAE) and standard deviation (STD) were used to

311 quantify the accuracy and uncertainty of CRC, which were calculated in Eqs. 9 and 10.

312
$$MAE^k = \frac{\sum_{i=1}^{n}|CRC_{s,i}^k - CRC_o^k|}{n} \tag{9}$$

313
$$STD^k = \sqrt{\frac{\sum_{i=1}^{n}(CRC_{s,i}^k - \overline{CRC_s^k})^2}{n}} \tag{10}$$

314 where, n is the number of behavioral parameter sets, and superscript k indicates the runoff

315 component (one of rainfall, snowmelt, glacier melt and baseflow). Subscript s and o indicate

316 the simulated and observed value (observed value is the CRC produced by the tri-objective

317 calibrated benchmark running). $CRC_{s,i}^k$ is the contribution of runoff component k simulated by

318 the parameter set i. $\overline{CRC_s^k}$ is the average CRC simulated by all the behavioral parameter sets.

319   In the remaining experiments in Table 3, the influence of isotope data availability on model

320 performance were quantified by changes in model performance in the validation period and

321 internal validate hydrological stations, as well as the uncertainty of CRC estimated by Eq. 10.

322

323   **3. Results**

324   **3.1 Performance of the tracer-aided hydrological model**

325   Figure 2 shows performance of the benchmark model running (i.e., BM_YTR scenario in

326   Table 3) forced and calibrated by the full available isotope dataset. Seasonal variations in

327   discharge and SCA were reproduced well by the bi-objective calibration (Figure 2a and 2b),

328   indicated by the high values of NSE_{dis} (>0.8) and $lnNSE_{dis}$ (>0.8), and a low $RMSE_{SCA}$ (<0.08).

329   The peak flows were less well reproduced by the model in comparison to the simulation of

330   baseflow processes, partly due to the inaccurate precipitation input data at the high altitudes.

331   The model showed extremely poor performance for the simulation of stream water isotope

332   when looking at the large uncertainty range (Figure 2c) and low NSE_{iso} (-0.72). The tri-objective

333   calibration significantly improved the isotope simulation (Figure 2f), without bringing much

334   sacrifice to the performance in simulating discharge and SCA (considering the minimum values

335   of NSE_{dis} and $lnNSE_{dis}$ are around 0.7 in Figure 2d and 2e). Moreover, the tri-objective

336   calibration slightly reduced uncertainty for simulation of the rising hydrograph in the 2009

337   spring (Figure 2d). The seasonal variations in stream water $\delta^{18}O$ were captured well at all the

338   four stations by simulations from the tri-objective calibration. The mean contributions of

339   rainfall and snowmelt to annual streamflow estimated by the bi-objective calibration were 62.8%

340   and 10.8%, which were around 1%-7% smaller than those estimated by the tri-objective

341   calibration (Table 4). In contrast, the contribution of glacier melt estimated by the tri-objective

342   calibration (17.1%) was lower than that estimated by the bi-objective calibration (26.4%).

343   Surface runoff which was mainly fed by glacier melt in the YTR showed a larger proportion in

344   the total streamflow simulated by a bi-objective calibration (52.1%) than that in the simulation

345   of a tri-objective calibration (44.7%), while baseflow contribution quantified by the bi-

346   objective calibration is smaller. Standard deviation values of the quantified CRCs indicated that

347   the tri-objective calibration estimated smaller uncertainties for the quantifications of runoff

348   components. A benchmark parameter set that performed well on multiple objectives was

349   selected among the behavioral parameters of BM_YTR calibrated by tri-objective method (as

350   shown in Table 5), to produce stream water $\delta^{18}O$ for model calibration in experiment 3 in YTR

351   basin.

352   **[Figure 2]**

353   **[Table 4]**

354   **[Table 5]**

355   Figure 3 shows model performances in the KR catchment. Variations of discharge and SCA

356   were reproduced comparably well by the bi- and tri-objective calibrations indicated by the

357   similar metric values. However, the bi-objective calibration produced extremely poor

358   performance for the isotope simulation with low NSE_{iso} and a large simulation error of ~5‰

359 (Figure 3c). The tri-objective calibration captured the seasonal variations in stream water δ^{18}O

360 during the study period well. Similarly to YTR, the tri-objective calibration resulted in lower

361 uncertainty in the simulated hydrograph (e.g., early 2010, 2006 and 2008), benefiting from

362 involving isotope for the model calibration to reject parameter sets that produced good

363 performance for discharge and SCA simulations but poor performance for isotope simulation.

364 Regarding the CRCs to total streamflow, the bi-objective and tri-objective calibrations

365 estimated similar results with differences up to 3%. The mean contributions of rainfall,

366 snowmelt and glacier melt to annual streamflow in the KR catchment were around 45%, 22%

367 and 33%, respectively. Contribution of surface runoff estimated by the bi-objective calibration,

368 however, was 13% lower than that estimated by the tri-objective calibration. In contrast,

369 baseflow is more important in the total streamflow simulated by the bi-objective calibration

370 (accounting for 38%) in comparison to the simulation of the tri-objective calibration

371 (accounting for 25%). Again in the KR catchment, uncertainties of CRCs quantified by the tri-

372 objective calibration are much smaller than those estimated by the bi-objective calibration

373 (Figure 3).

374 **[Figure 3]**

375 **3.2 Changes in model simulations forced by different assumed glacier meltwater isotopes**

376 Model simulations forced by assumed glacier meltwater δ^{18}O that are 5‰ (scenario

377 BM_YTR, Δ_δ=5‰) and 7‰ (scenario G_Δ7, Δ_δ=7‰) lower than the long-term average

378 precipitation δ^{18}O showed the best discharge simulations in the validation period (2011-2015)

379 and stations (Yangcun and Nugesha), indicated by the high average metric values (Figure 4). It

380 is noted that simulations of all the glacier meltwater isotope input scenarios in experiment 1

381 except G_Δ1 performed better than the bi-objective calibration in which isotope data was not

382 involved for parameter identification. Discharge simulation in the scenario of G_Δ1 estimated

383 higher performance in the validation period than the bi-objective calibration (Figure 4a), but

384 lower performance at internal stations (Figure 4b and 4c).

385 **[Figure 4]**

386 Figure 5 shows the average CRCs and corresponding uncertainties estimated by the

387 different glacier melt isotope inputs. Scenarios with larger Δ_δ values (i.e., glacier meltwater

388 isotope is much lower than precipitation isotope) tended to result in higher contributions of

389 precipitation and lower contributions of glacier melt (Figure 5). This can be expected, as stream

390 water δ^{18}O is a mixture mainly from δ^{18}O of precipitation and glacier meltwater in YTR basin

391 and precipitation δ^{18}O is fixed in all the scenarios. Result of scenario G_Δ1, however, estimated

392 a smaller contribution of glacier melt than the scenario G_Δ3. This was likely due to that the

393 behavioral parameter sets were selected based on the performance of both discharge and isotope

394 simulations. Parameter sets that estimated higher glacier melt contribution with good

395   performance in isotope simulation but performed poorly on discharge simulation were excluded

396   from the behavioral set in the G_Δ1 scenario.

397   **[Figure 5]**

398   **3.3 Changes in model performance forced by corrected isoGSM product using different**

399   **site measurements of precipitation isotope**

400   While different scenarios produced similar SCA simulations in the validation period

401   (Figure 6d), the performance of discharge simulation significantly differed among the

402   precipitation isotope input scenarios in experiment 2. In scenarios BM_YTR and P_2stationNL,

403   the model performed better than the bi-objective calibration in the validation period (Figure 6a)

404   and stations (Figure 6b and 6c), showing higher average values and smaller ranges of NSE_{dis},

405   which indicated that the model benefitted from involving isotope data for calibration. The

406   model performance forced by scenario P_2stationNY was close to that of the bi-objective

407   calibration. Using precipitation isotope input from the scenario P_1station, however, the model

408   performance was significantly worse than that of the bi-objective calibration. Reasons for the

409   variable model performance forced by the precipitation isotope input scenarios could be: Site

410   measurements of precipitation isotope used in scenarios BM_YTR (using data at four sampling

411   stations) and P_2stationNL (using data at the most downstream sampling station and the most

412   upstream sampling station) tended to provide more informative spatial distribution of

413   precipitation $\delta^{18}O$ in the basin and were the most valuable data for the correction of isoGSM

414   estimate; in the scenario of P_1station, on the contrary, the isoGSM product was inadequately

415   corrected by site precipitation isotope measured only at the most downstream station Nuxia,

416   resulting in much errors in the isoGSM product at high altitudes.

417   **[Figure 6]**

418   Figure 7 shows the average CRCs and corresponding uncertainties estimated by the

419   different precipitation isotope input scenarios. All scenarios produced lower uncertainties than

420   the bi-objective calibration, which can be expected as they were calibrated by a tri-objective

421   approach. The variable precipitation input scenarios resulted in contribution differences of

422   around 10% in runoff components of rainfall, glacier melt and baseflow. Different site

423   measurements of precipitation isotope that were used for the correction of isoGSM product

424   resulted in different altitudinal lapse rates in the corrected isoGSM input (i.e., parameter *a* in

425   equation 2); and scenario P_1station estimated the most overestimated average precipitation

426    $\delta^{18}O$ ($\overline{\delta^{18}O_{precipitation}}$), while scenario P_2stationNL estimated the lowest $\overline{\delta^{18}O_{precipitation}}$,

427   leading to varied precipitation contributions to streamflow.

428   **[Figure 7]**

429   Among the evaluation metrics, discharge simulation at Nugesha station showed the largest

430   sensitivity to precipitation isotope inputs. As shown in Figure 8, scenarios P_2stationNY and

431   P_1station estimated higher contribution of meltwater, earlier discharge onset timing and higher

432   peak flow. The discharge began to rise especially early (around February) in scenario P_1station,

433   because of the low calibrated value for the melting temperature threshold T_0 (-4.5°C), resulted

434   in extremely poor discharge simulation (average NSE is around 0, Figure 8d).

435   **[Figure 8]**

436   **3.4 Model performance constrained by different stream water sampling strategies**

437   Figure 9 shows the accuracy and uncertainty metrics of CRCs produced by experiment 3

438   in the YTR basin. In comparison to the baseline scenario of RT_TYR_BM, collecting stream

439   isotope data in the dry season (i.e., from November to next February in scenario

440   RT_YTR_WholeYear) brought little benefits to the estimation of water sources proportions, but

441   significantly improved the quantifications of runoff generation pathways indicated by the lower

442   MAE and STD in Figure 9b. The stream water in dry season was fed mainly by groundwater.

443   Stream water isotope data collected in this period reflect the release of groundwater storage,

444   thus helping to constrain the partition between surface and subsurface runoff pathway. On the

445   other hand, reducing the frequency of stream isotope data from weekly to monthly (i.e., scenario

446   RT_YTR_Monthly) led to significantly higher MAE and STD for both the partitions of water

447   sources and runoff pathways, which indicated that stream water isotope data collected by a

448   monthly sampling strategy could provide less constrains to model calibration. Extending the

449   duration of stream isotope sampling period by one or two years (i.e., scenarios RT_YTR_2year

450   and RT_YTR_3year) did not bring much benefits to the quantifications of CRCs regarding the

451   similar metric values. Using stream water isotope data from a three years' sampling

452   (RT_YTR_3year) even led to higher MAE and STD than that using stream water isotope data

453   from a 2 years' sampling (RT_YTR_2year), which might be an occasional result obtained by

454   the random calibration procedure (100 pySOT runs). In comparison to simulations constrained

455   by stream water isotope data from multiple sampling years, results constrained by stream water

456   isotope data from multiple sampling sits (i.e., scenarios of RT_YTR_2station and

457   RT_YTR_4station) yielded lower MAE and STD for the quantified CRCs.

458   **[Figure 9]**

459   Model simulations calibrated by spatially distributed stream δ^{18}O data collected in a one-

460   time field campaign reduced the CRC uncertainty compared to the bi-objective calibration

461   (Figure 9). However, its MAE and STD for the quantifications of CRCs were higher than that

462   estimated by the model when calibrated by weekly sampled time series of stream δ^{18}O.

463   Additionally using stream isotope data from four major tributaries (i.e., scenario

464   RS_YTR_Tributary) brought little benefits to the model performance than using isotope data

465   from the main stream solely (RS_YTR_Main), partly due to the signatures of stream water

466   isotope from tributaries were already reflected by water samples collected at confluences on

467   the main river channel.

468   In the KR catchment, stream isotope data was collected from five continues years,

469   providing better data basis for the evaluation of the influence of sampling period duration.

470   Figure 10 and 11 compare the CRC estimations and their uncertainty metric STD of variable

471   scenarios. For the estimate of water sources, the model produced rather large uncertainty ranges

472   of ~20% and ~40% for the contributions of rainfall and glacier melt when calibrating the model

473   using discharge and SCA. Using one-year's stream water isotope data for model calibration,

474   the uncertainty ranges were reduced by rejecting some outliers as shown in Figure 10a-c, but

475   the STD was still large (Figure 11). The STD can be reduced by increasing the number of

476   calibration isotope data at a rate of ~1%/year. Using isotope data collected from five years,

477   however, didn't result in further decrease in the CRC uncertainties compared to the result

478   calibrated by isotope data collected in a four-year sampling period. The situation, however, was

479   quite different for the estimates of runoff pathways. The bi-objective calibration produced a

480   large uncertainty of ~40% and a STD of ~10% (Figure 10d) for the contribution of baseflow.

481   Using one-year's data for model calibration, the uncertainty range was significantly reduced by

482   about half of that modelled by the bi-objective calibration (from ~10% to ~5%). However,

483   further increase in the duration of sampling period did not bring much improvements on

484   constraining the uncertainties in quantifications of runoff pathways with STD fluctuating

485   around only 4%. It is indicated that model calibration upon more stream isotope data was useful

486   to better constrain the uncertainties of the model simulations and modeled CRCs, but benefit

487   would disappear after a certain duration of stream water sampling period has been reached.

488   **[Figure 10]**

489   **[Figure 11]**

490   **4. Discussions**

491   **4.1 Implications for water sampling for isotope analysis in high mountains of TP**

492   This study tested the reliance of the benefits of using tracer-aided hydrological model on

493   isotope data availability in two mountainous catchments YTR and KR on the TP. Our findings

494   consistently showed that the model robustness, with respect to performance in the validation

495   period and internal stations and the quantifications of CRCs, can be significantly improved by

496   involving isotope data for parameter calibration, similarly to previous tracer-aided modeling

497   studies (e.g., He et al., 2019; Ala-aho et al., 2017; Birkel et al., 2010). It can be expected that

498   more data help to provide more constrains on identification of model parameters. Nonetheless,

499   water sampling in high mountains on the TP is restricted by environment accessibility, financial

500   and human costs (Stevenson et al., 2021, Li et al., 2020). It is therefore highly needed to find

501   optimal strategies of collecting water samples that balance well between data adequacy for

502   model running and affordable sampling cost (Sprenger et al., 2019).

503   As an important water source in mountainous catchment on the TP, sampling of glacier

504   meltwater was expected to be favorable for the determination of glacier meltwater isotopic

505   composition and its contribution to total streamflow (He et al., 2019). Field campaign for

506   sampling of glacier melt water is strongly challenging in the YTR basin in this study, due to the

507   harsh accessibility of very high altitudes where glaciers lie. We thus assumed that glacier

508   meltwater $\delta^{18}O$ was lower than the average local precipitation $\delta^{18}O$ by an offset parameter (Δ_δ).

509   This simple assumption turned to work well on driving the tracer-aided hydrological model and

510   produced better performance than the bi-objective calibration in both validation periods and

511   internal stations. Experiments by using different Δ_δ values indicated that the prior assumed

512   isotopic compositions of glacier melt have small influence on the estimated glacier meltwater

513   contribution in the YTR basin. The Δ_δ values ranging from 2‰-9‰ led to only ~5% difference

514   in the estimated contributions of glacier melt. Using a Δ_δ to estimate glacier meltwater $\delta^{18}O$

515   could serve as an option to force the tracer-aided hydrological models in high-mountain

516   catchments where collecting glacier meltwater samples is highly challenging.

517   Results of experiment 2 indicated that the original isoGSM precipitation $\delta^{18}O$ data showed

518   large bias in the high mountain basins on TP, and must undergo correction before using to force

519   the tracer-aided hydrological model. Our experiments showed that measurement of

520   precipitation isotope at only two sampling sites (scenario P_2stationNL) in the large YTR basin

521   of 2×10^5 km^2 can be highly valuable for the correction of isoGSM product. Forced by isoGSM

522   data that was corrected by precipitation $\delta^{18}O$ measurements from two sampling sites, the model

523   performed better than the bi-objective calibration in simulating discharge in the validation

524   period and internal stations, and performed comparably to the simulations of a benchmark

525   running which used precipitation $\delta^{18}O$ measurements from four stations for the isoGSM

526   correction. This benefitted from the large altitudinal range covered by the two sampling sites (a

527   most downstream site Nuxia and a most upstream site Lazi) to represent the spatial pattern of

528   isoGSM bias. Likewise using measurement data at two sites in the scenario P_2stationNY,

529   model performance deteriorated visibly, as the sampling sites (Nuxia and Yangchun) were both

530   located in the downstream regions, being worse at representing the spatial pattern of

531   precipitation $\delta^{18}O$ over the basin. Consequently, the strategy of collecting precipitation samples

532   to correct isoGSM should be carefully designed; spending high cost on collecting precipitation

533   samples within a small region might be not worth at improving the performance of the tracer-

534   aided hydrological model.

535   Measurements of stream water $\delta^{18}O$ are essential for the calibration and evaluation of

536   tracer-aided hydrological models. Three kinds of sampling strategies in YTR basin were

537   evaluated in experiment 3: one-time campaign field sampling, continuous sampling at a fixed

538   location for a long period, and continuous sampling at multiple fixed locations during a short
539   period. It is indicated that continuously sampled stream water $\delta^{18}O$ at a fix location is more
540   valuable for aiding hydrological model than that collected by one-time field sampling
541   campaigns at distributed sites. Seasonality of stream water $\delta^{18}O$ referring to the processes of
542   water storage, mixture and transport in the basin can be better captured by continuous time
543   series measurements of $\delta^{18}O$ data (McGuire and McDonnell, 2006). Spatially sampled stream
544   water $\delta^{18}O$ data by one-time field sampling campaigns possibly miss seasonal $\delta^{18}O$ signatures
545   of stream water that were caused by seasonal runoff generation processes (Kendall and Coplen,
546   2001; Nan et al., 2019), and provide less constrains for the model calibration. Sampling of
547   stream water during dry season (scenario RT_YTR_WholeYear) brought little improvements
548   to the modeling of water source proportions, which is consistent with the findings in Stevenson
549   et al. (2021). High frequent like weekly sampling of stream water in the dry season makes small
550   senses on improving the stream $\delta^{18}O$ data quality, as stream $\delta^{18}O$ in this season has little
551   variations due to small precipitation triggered runoff inputs. Monthly sampling of stream water
552   (RT_YTR_Monthly) turned to be insufficient to capture the strong hydrological variations in
553   the wet season (Birkel and Soulsby, 2015). For large basins like YTR, increasing the number
554   of sampling site for stream water $\delta^{18}O$ is more useful than extending the years of sampling
555   period at fixed sites, as seasonality of $\delta^{18}O$ signatures of water sources should be similar among
556   years in a short study period. Consequently, continuous sampling at multiple locations in a short
557   period like one or two years seems to be the optimal stream sampling strategy for running
558   tracer-aided hydrological model in mountainous basins like YTR on the TP. The value of
559   extending sampling period was more significant in a smaller catchment KR. The uncertainty of
560   CRC estimation kept decreasing until the data series length reached four years and two years,
561   for the aspects of water source and runoff pathway, respectively. This was consistent with the
562   finding by Stevenson et al. (2021) that the benefits from isotope plateaued after a certain year
563   number, which was five for that study.

4.2 Uncertainties and limitations

565   This study used simulated stream $\delta^{18}O$ of a benchmark model running to represent the fully
566   available dataset of stream $\delta^{18}O$ for water sampling in the YTR basin, due to the limited stream
567   water samples. This procedure likely caused the inherent correlation of the stream $\delta^{18}O$ dataset,
568   which made the model easily reproduce the assumed measurements of stream $\delta^{18}O$ and may
569   underestimate the value of stream $\delta^{18}O$ data collected in extended sampling years and sampling
570   sites. Results in this study serve to provide preliminary understandings of the influences of
571   stream water sampling strategy on the model performance. More solid evaluations, however,
572   can be further benefited from using more real field measurements of stream $\delta^{18}O$ in the
573   mountain basins.

574   Our study tried to look for optimal water sampling strategies to provide isotope input and
575   calibration data for the tracer-aided hydrological model in the YTR basin and KR catchment on
576   the TP. The transferability of our findings to other basins can be partly expected. For example,
577   we can expect that in catchments where precipitation $\delta^{18}O$ and runoff processes show small
578   spatial heterogeneity, collecting water samples at multiple stations would bring few additional
579   benefits for the modeling work than collecting water samples at a sole station. The influence of
580   assumed glacier meltwater would differ with the glacier covered area fraction in the basins.
581   However, situations in catchments with different geographical and climatic characteristics were
582   not evaluated in this study, which is restricted by the fact that high-quality water isotope data
583   in a set of mountain basins on the TP were hardly available currently (Birkel and Soulsby, 2015).
584   The authors suggest tracer-aided modeling researchers to publish their water isotope data to
585   improve the evaluation of the reliance of tracer-aided modeling performance on water sampling
586   strategy (similarly to He et al. 2021; Niinikoski et al., 2016; Yde et al., 2016).

587   **5. Conclusion**

588   The value of water isotope data for aiding hydrological modeling in large mountainous
589   catchments was tested by a set of numerical experiments in the YTR basin. Reliance of the
590   tracer-aided model performance on the availability of input isotope data and evaluation stream
591   water isotope data was extensively investigated in the numerical experiments. Results could
592   provide important guidance for water sampling in mountainous regions on the TP. Our main
593   finds are as follows:

594   1. In high-mountain basins where glacier meltwater samples for isotope analysis are not
595   available, estimating isotopic composition of glacier meltwater by an offset parameter from
596   precipitation isotope is a feasible way to force the tracer-aided hydrological model. Our test
597   indicated that using a set of glacier meltwater $\delta^{18}O$ that are 2‰~9‰ lower than the mean
598   precipitation $\delta^{18}O$, resulted in small changes in the model performance and the quantifications
599   of CRCs (smaller than 5%) in the YTR basin. This influence, however, is expected to change
600   with the glacier area coverages in other mountain basins.

601   2. Strategy of field sampling for precipitation to correct the isoGSM product should be
602   carefully designed. Collecting precipitation samples at sites from the same altitude tends to be
603   worse at representing the spatial pattern of precipitation $\delta^{18}O$ over the basin than collecting
604   precipitation samples from sites covering a range of altitudes. Measurements of precipitation
605   isotope at only two sampling sites covering an elevation range of 2900-6900m in the large YTR
606   basin of 2×10^5 km^2 can be highly valuable for the correction of isoGSM product.

607   3. Colleting weekly stream water samples at multiple sites in the wet and warm seasons is
608   the optimal strategy for calibrating and evaluating a tracer-aided hydrological model in the YTR
609   basin. It is highly recommended to increase the number of stream water sampling sites in the

610 high-mountain basins rather than extending the duration of sampling period at a sole site.
611 Benefits from extending the duration of sampling period is more visible in a small catchment
612 but smaller in large basins, and tend to disappear when a certain duration of sampling period
613 has been reached.
614

Code and data availability

616 Code and data availability. The isotope data and the code of THREW-T model used in this study
617 are available from the corresponding author (tianfq@tsinghua.edu.cn). Other data sets and the
618 calibration program pySOT are publicly available as follows: DEM
619 (http://www.gscloud.cn/sources/details/310?pid=302, last access: 1 January 2019, Geospatial
620 Data Cloud Site, 2019), CMFD (https://doi.org/10.11888/AtmosphericPhysics.tpe.249369.file,
621 Yang and He, 2019), glacier data (https://doi.org/10.3972/glacier.001.2013.db, Liu et al., 2012),
622 NDVI (https://doi.org/10.5067/MODIS/MOD13A3.006, Didan et al., 2015), LAI
623 (https://doi.org/10.5067/MODIS/MOD15A2H.006, Myneni et al., 2015), HWSD
624 (https://data.tpdc.ac.cn/zh-hans/data/3519536a-d1e7-4ba1-8481-6a0b56637baf/?q=HWSD,
625 last access: 1 January 2019, He, 2019) and the pySOT program
626 (https://doi.org/10.5281/zenodo.569554, Eriksson et al., 2017). These data sets and programs
627 are also referred to in the main text (Yang et al., 2010; Chen et al., 2018).

Author contribution

629 YN, ZH and FT conceived the idea; ZW provided the isoGSM data; LT provided the
630 measurement isotope data; YN, ZH and FT conducted analysis; ZW and LT provided comments
631 on the analysis; all the authors contributed to writing and revisions.

Financial support

633 This study has been supported by the National Natural Science Foundation of China (grant no.
634 92047301).

Competing interests

636 At least one of the (co-)authors is a member of the editorial board of Hydrology and Earth
637 System Sciences.
638

References

640 Ala-aho, P., Tetzlaff, D., McNamara, J. P., Laudon, H., and Soulsby, C.: Using isotopes to
641 constrain water flux and age estimates in snow-influenced catchments using the STARR
642 (Spatially distributed Tracer-Aided Rainfall–Runoff) model, Hydrology and Earth System
643 Sciences, 21, 5089-5110, 10.5194/hess-21-5089-2017, 2017.

Birkel, C., Dunn, S. M., Tetzlaff, D., and Soulsby, C.: Assessing the value of high-resolution isotope tracer data in the stepwise development of a lumped conceptual rainfall-runoff model, Hydrological Processes, 24, 2335-2348, 10.1002/hyp.7763, 2010.

Birkel, C., Tetzlaff, D., Dunn, S. M., and Soulsby, C.: Using time domain and geographic source tracers to conceptualize streamflow generation processes in lumped rainfall-runoff models, Water Resources Research, 47, 10.1029/2010wr009547, 2011.

Birkel, C., and Soulsby, C.: Advancing tracer-aided rainfall-runoff modelling: a review of progress, problems and unrealised potential, Hydrological Processes, 29, 5227-5240, 10.1002/hyp.10594, 2015.

Bloeschl, G., and Montanari, A.: Climate change impact: throwing the dice?, Hydrological Processes, n/a-n/a, 10.1002/hyp.7574, 2009.

Boral, S., and Sen, I. S.: Tracing 'Third Pole' ice meltwater contribution to the Himalayan rivers using oxygen and hydrogen isotopes, Geochemical Perspectives Letters, 48-53, 10.7185/geochemlet.2013, 2020.

Bowen, G. J., Cai, Z., Fiorella, R. P., and Putman, A. L.: Isotopes in the Water Cycle: Regional-to Global-Scale Patterns and Applications, in: Annual Review Of Earth And Planetary Sciences, Vol 47, edited by: Jeanloz, R., and Freeman, K. H., Annual Review of Earth and Planetary Sciences, 453-+, 2019.

Capell, R., Tetzlaff, D., and Soulsby, C.: Can time domain and source area tracers reduce uncertainty in rainfall - runoff models in larger heterogeneous catchments?, Water Resources Research, 48, 10.1029/2011wr011543, 2012.

Chen, X., Long, D., Hong, Y., Zeng, C., and Yan, D.: Improved modeling of snow and glacier melting by a progressive two-stage calibration strategy with GRACE and multisource data: How snow and glacier meltwater contributes to the runoff of the Upper Brahmaputra River basin?, Water Resources Research, 53, 2431-2466, 10.1002/2016wr019656, 2017.

Chen, X., Long, D., Liang, S., He, L., Zeng, C., Hao, X., and Hong, Y.: Developing a composite daily snow cover extent record over the Tibetan Plateau from 1981 to 2016 using multisource data, Remote Sen. Environ., 215, 284–299, https://doi.org/10.1016/j.rse.2018.06.021, 2018.

Delavau, C. J., Stadnyk, T., and Holmes, T.: Examining the impacts of precipitation isotope input on distributed, tracer-aided hydrological modelling, Hydrology and Earth System Sciences, 21, 2595-2614, 10.5194/hess-21-2595-2017, 2017.

Didan, K.: MOD13A3 MODIS/Terra vegetation Indices Monthly L3 Global 1km SIN Grid V006, NASA EOSDIS Land Processes DAAC [data set], https://doi.org/10.5067/MODIS/MOD13A3.006, 2015.

Dong, G., Weng, B., Chen, J., Yan, D., and Wang, H.: Variation characteristics of stable isotopes in water along main stream of Naqu River in source area of Nujiang River, Water

681   Resources and Hydropower Engineering, 49, 108-114, 2018.

682   Duethmann, D., Bolch, T., Farinotti, D., Kriegel, D., Vorogushyn, S., Merz, B., Pieczonka, T.,

683   Jiang, T., Su, B., and Guentner, A.: Attribution of streamflow trends in snow and glacier

684   melt-dominated catchments of the Tarim River, Central Asia, Water Resources Research,

685   51, 4727-4750, 10.1002/2014wr016716, 2015.

686   Dunn, S. M., McDonnell, J. J., and Vaché, K. B.: Factors influencing the residence time of

687   catchment waters: A virtual experiment approach, Water Resources Research, 43,

688   10.1029/2006wr005393, 2007.

689   Eriksson, D., Bindel, D., and Shoemaker, C.: Dme65/Pysot: V0.1.35, Zenodo [code],

690   https://doi.org/10.5281/zenodo.569554, 2017.

691   Gao J., Tian L., and Liu, Y.: Oxygen isotope variation in the water cycle of the Yamzho Lake

692   Basin in southern Tibetan Plateau, Chinese Sci. Bull., 54, 2758–2765, 2009.

693   Gupta, H. V., Wagener, T., and Liu, Y.: Reconciling theory with observations: elements of a

694   diagnostic approach to model evaluation, Hydrological Processes, 22, 3802-3813,

695   10.1002/hyp.6989, 2008.

696   He, Y.: Pan-TPE soil map based on Harmonized World Soil Database (V1.2), National Tibetan

697   Plateau Data Center [data set], https://data.tpdc.ac.cn/zh-hans/data/3519536a-d1e7-4ba1-

698   8481-6a0b56637baf/?q=HWSD, 2019

699   He, Z. H., Tian, F. Q., Gupta, H. V., Hu, H. C., and Hu, H. P.: Diagnostic calibration of a

700   hydrological model in a mountain area by hydrograph partitioning, Hydrology and Earth

701   System Sciences, 19, 1807-1826, 10.5194/hess-19-1807-2015, 2015.

702   He, Z., Unger-Shayesteh, K., Vorogushyn, S., Weise, S. M., Kalashnikova, O., Gafurov, A.,

703   Duethmann, D., Barandun, M., and Merz, B.: Constraining hydrological model parameters

704   using water isotopic compositions in a glacierized basin, Central Asia, Journal of

705   Hydrology, 571, 332-348, 10.1016/j.jhydrol.2019.01.048, 2019.

706   He, Z., Unger-Shayesteh, K., Vorogushyn, S., Weise, S. M., Duethmann, D., Kalashnikova, O.,

707   Gafurov, A., and Merz, B.: Comparing Bayesian and traditional end-member mixing

708   approaches for hydrograph separation in a glacierized basin, Hydrology and Earth System

709   Sciences, 24, 3289-3309, 10.5194/hess-24-3289-2020, 2020.

710   He, Z., Duethmann, D., and Tian, F.: A meta-analysis based review of quantifying the

711   contributions of runoff components to streamflow in glacierized basins, Journal of

712   Hydrology, 603, 126890, 10.1016/j.jhydrol.2021.126890, 2021.

713   Hindshaw, R. S., Tipper, E. T., Reynolds, B. C., Lemarchand, E., Wiederhold, J. G., Magnusson,

714   J., Bernasconi, S. M., Kretzschmar, R., and Bourdon, B.: Hydrological control of stream

715   water chemistry in a glacial catchment (Damma Glacier, Switzerland), Chemical Geology,

716   285, 215-230, 10.1016/j.chemgeo.2011.04.012, 2011.

717   Immerzeel, W. W., van Beek, L. P. H., and Bierkens, M. F. P.: Climate Change Will Affect the

718   Asian Water Towers, Science, 328, 1382-1385, 10.1126/science.1183188, 2010.

719   Jeelani, G., Shah, R. A., Jacob, N., and Deshpande, R. D.: Estimation of snow and glacier melt
720   contribution to Liddar stream in a mountainous catchment, western Himalaya: an isotopic
721   approach,   Isotopes   in   environmental   and   health   studies,   53,   18-35,
722   10.1080/10256016.2016.1186671, 2017.

723   Kendall, C., and Coplen, T. B.: Distribution of oxygen-18 and deuterium in river waters across
724   the United States, Hydrological Processes, 15, 1363-1393, 10.1002/hyp.217, 2001.

725   Klaus, J., and McDonnell, J. J.: Hydrograph separation using stable isotopes: Review and
726   evaluation, Journal of Hydrology, 505, 47-64, 10.1016/j.jhydrol.2013.09.006, 2013.

727   Knapp, J. L. A., Neal, C., Schlumpf, A., Neal, M., and Kirchner, J. W.: New water fractions and
728   transit time distributions at Plynlimon, Wales, estimated from stable water isotopes in
729   precipitation and streamflow, Hydrology and Earth System Sciences, 23, 4367-4388,
730   10.5194/hess-23-4367-2019, 2019.

731   Kong, Y., Wang, K., Pu, T., and Shi, X.: Nonmonsoon Precipitation Dominates Groundwater
732   Recharge Beneath a Monsoon‐Affected Glacier in Tibetan Plateau, Journal of Geophysical
733   Research: Atmospheres, 124, 10913-10930, 10.1029/2019jd030492, 2019.

734   Laudon, H., Taberman, I., Ågren, A., Futter, M., Ottosson-Löfvenius, M., and Bishop, K.: The
735   Krycklan Catchment Study-A flagship infrastructure for hydrology, biogeochemistry, and
736   climate research in the boreal landscape, Water Resources Research, 49, 7154-7158,
737   10.1002/wrcr.20520, 2013.

738   Li, Z.-J., Li, Z.-X., Song, L.-L., Gui, J., Xue, J., Zhang, B. J., and Gao, W. D.: Hydrological
739   and runoff formation processes based on isotope tracing during ablation period in the
740   source regions of Yangtze River, Hydrology and Earth System Sciences, 24, 4169-4187,
741   10.5194/hess-24-4169-2020, 2020.

742   Li, Z., Feng, Q., Li, Z., Yuan, R., Gui, J., and Lv, Y.: Climate background, fact and hydrological
743   effect of multiphase water transformation in cold regions of the western china: a review,
744   EARTH ENCE REVIEWS, 190, 33-57, https://doi.org/10.1016/j.earscirev.2018.12.004,
745   2019.

746   Liu, S.: The second glacier inventory dataset of China (version 1.0) (2006–2011), National
747   Tibetan Plateau Data Center [data set], https://doi.org/10.3972/glacier.001.2013.db, 2012.

748   Liu, Z., Tian, L., Yao, T., Gong, T., Yin, C., and Yu, W.: Temporal and spatial variations of delta
749   O-18 in precipitation of the Yarlung Zangbo River Basin, J. Geogr. Sci., 17, 317–326,
750   https://doi.org/10.1007/s11442-007-0317-1, 2007.

751   Lutz, A. F., Immerzeel, W. W., Shrestha, A. B., and Bierkens, M. F. P.: Consistent increase in
752   High Asia's runoff due to increasing glacier melt and precipitation, Nature Climate Change,
753   4, 587-592, 10.1038/nclimate2237, 2014.

754   McGuire, K. J., and McDonnell, J. J.: A review and evaluation of catchment transit time

755   modeling, Journal of Hydrology, 330, 543-563, 10.1016/j.jhydrol.2006.04.020, 2006.

756   McGuire, K. J., Weiler, M., and McDonnell, J. J.: Integrating tracer experiments with modeling

757   to assess runoff processes and water transit times, Advances in Water Resources, 30, 824-

758   837, 10.1016/j.advwatres.2006.07.004, 2007.

759   Myneni, R., Knyazikhin, Y., and Park, T.: MOD15A2H MODIS/Terra Leaf Area Index/FPAR

760   8-Day L4 Global 500m SIN Grid V006, NASA EOSDIS Land Processes DAAC [data set],

761   https://doi.org/10.5067/MODIS/MOD15A2H.006, 2015.

762   Nan, Y., Tian, F., Hu, H., Wang, L., and Zhao, S.: Stable Isotope Composition of River Waters

763   across the World, Water, 11, 1760, 10.3390/w11091760, 2019.

764   Nan, Y., He, Z., Tian, F., Wei, Z., and Tian, L.: Can we use precipitation isotope outputs of

765   isotopic general circulation models to improve hydrological modeling in large

766   mountainous catchments on the Tibetan Plateau?, Hydrology and Earth System Sciences,

767   25, 6151-6172, 10.5194/hess-25-6151-2021, 2021b.

768   Nan, Y., Tian, L., He, Z., Tian, F., and Shao, L.: The value of water isotope data on improving

769   process understanding in a glacierized catchment on the Tibetan Plateau, Hydrology and

770   Earth System Sciences, 25, 3653-3673, 10.5194/hess-25-3653-2021, 2021a.

771   Niinikoski, P. I. A., Hendriksson, N. M., and Karhu, J. A.: Using stable isotopes to resolve

772   transit times and travel routes of river water: a case study from southern Finland, Isotopes

773   in environmental and health studies, 52, 380-392, 10.1080/10256016.2015.1107553, 2016.

774   Ohlanders, N., Rodriguez, M., and McPhee, J.: Stable water isotope variation in a Central

775   Andean watershed dominated by glacier and snowmelt, Hydrology and Earth System

776   Sciences, 17, 1035-1050, 10.5194/hess-17-1035-2013, 2013.

777   Pomeroy, J. W., Gray, D. M., Brown, T., Hedstrom, N. R., Quinton, W. L., Granger, R. J., and

778   Carey, S. K.: The cold regions hydrological model: a platform for basing process

779   representation and model structure on physical evidence, Hydrological Processes, 21,

780   2650-2667, 10.1002/hyp.6787, 2007.

781   Rai, S. P., Singh, D., Jacob, N., Rawat, Y. S., Arora, M., and BhishmKumar: Identifying

782   contribution of snowmelt and glacier melt to the Bhagirathi River (Upper Ganga) near

783   snout of the Gangotri Glacier using environmental isotopes, Catena, 173, 339-351,

784   10.1016/j.catena.2018.10.031, 2019.

785   Reggiani, P., Hassanizadeh, S. M., Sivapalan, M., and Gray, W. G.: A unifying framework for

786   watershed thermodynamics: constitutive relationships, Advances In Water Resources, 23,

787   15-39, 10.1016/s0309-1708(99)00005-6, 1999.

788   Son, K., and Sivapalan, M.: Improving model structure and reducing parameter uncertainty in

789   conceptual water balance models through the use of auxiliary data, Water Resources

790   Research, 43, 10.1029/2006wr005032, 2007.

791   Sprenger, M., Stumpp, C., Weiler, M., Aeschbach, W., Allen, S. T., Benettin, P., Dubbert, M.,

792   Hartmann, A., Hrachowitz, M., Kirchner, J. W., McDonnell, J. J., Orlowski, N., Penna, D.,
793   Pfahl, S., Rinderer, M., Rodriguez, N., Schmidt, M., and Werner, C.: The Demographics
794   of Water: A Review of Water Ages in the Critical Zone, Reviews Of Geophysics, 57, 800-
795   834, 10.1029/2018rg000633, 2019.
796   Stevenson, J. L., Birkel, C., Neill, A. J., Tetzlaff, D., and Soulsby, C.: Effects of streamflow
797   isotope sampling strategies on the calibration of a tracer-aided rainfall-runoff model,
798   Hydrological Processes, 35, 10.1002/hyp.14223, 2021.
799   Tan, H., Chen, X., Shi, D., Rao, W., Liu, J., Liu, J., Eastoe, C. J., and Wang, J.: Base flow in the
800   Yarlungzangbo River, Tibet, maintained by the isotopically-depleted precipitation and
801   groundwater discharge, The Science of the total environment, 759, 143510,
802   10.1016/j.scitotenv.2020.143510, 2021.
803   Tetzlaff, D., Birkel, C., Dick, J., Geris, J., and Soulsby, C.: Storage dynamics in
804   hydropedological units control hillslope connectivity, runoff generation, and the evolution
805   of catchment transit time distributions, Water Resour Res, 50, 969-985,
806   10.1002/2013WR014147, 2014.
807   Tian, F., Hu, H., Lei, Z., and Sivapalan, M.: Extension of the Representative Elementary
808   Watershed approach for cold regions via explicit treatment of energy related processes,
809   Hydrology And Earth System Sciences, 10, 619-644, 10.5194/hess-10-619-2006, 2006.
810   Tian, F., Xu, R., Nan, Y., Li, K., and He, Z.: Quantification of runoff components in the Yarlung
811   Tsangpo River using a distributed hydrological model, Advances in Water Science, 31,
812   324-336, 2020.
813   Tong, R., Parajka, J., Salentinig, A., Pfeil, I., Komma, J., Széles, B., Kubáň, M., Valent, P.,
814   Vreugdenhil, M., Wagner, W., and Blöschl, G.: The value of ASCAT soil moisture and
815   MODIS snow cover data for calibrating a conceptual hydrologic model, Hydrology and
816   Earth System Sciences, 25, 1389-1410, 10.5194/hess-25-1389-2021, 2021.
817   Viviroli, D., Weingartner, R., and Messerli, B.: Assessing the hydrological significance of the
818   world's mountains, Mountain Research And Development, 23, 32-40, 10.1659/0276-
819   4741(2003)023[0032:athsot]2.0.co;2, 2003.
820   Wang, C., Dong, Z., Qin, X., Zhang, J., Du, W., and Wu, J.: Glacier meltwater runoff process
821   analysis using δD and δ18O isotope and chemistry at the remote Laohugou glacier basin
822   in western Qilian Mountains, China, Journal of Geographical Sciences, 26, 722-734,
823   10.1007/s11442-016-1295-y, 2016.
824   Wang, Y., Wang, L., Zhou, J., Yao, T., Yang, W., Zhong, X., Liu, R., Hu, Z., Luo, L., Ye, Q.,
825   Chen, N., and Ding, H.: Vanishing Glaciers at Southeast Tibetan Plateau Have Not Offset
826   the Declining Runoff at Yarlung Zangbo, Geophysical Research Letters, 48,
827   10.1029/2021gl094651, 2021.
828   Wolfe, B. B., Karst-Riddoch, T. L., Hall, R. I., Edwards, T. W. D., English, M. C., Palmini, R.,

829   McGowan, S., Leavitt, P. R., and Vardy, S. R.: Classification of hydrological regimes of
830   northern floodplain basins (Peace–Athabasca Delta, Canada) from analysis of stable
831   isotopes (δ18O, δ2H) and water chemistry, Hydrological Processes, 21, 151-168,
832   10.1002/hyp.6229, 2007.

833   Xi, X.: A Review of Water Isotopes in Atmospheric General Circulation Models: Recent
834   Advances and Future Prospects, International Journal of Atmospheric Sciences, 2014, 1-
835   16, 10.1155/2014/250920, 2014.

836   Xia, X., Li, S., Wang, F., Zhang, S., Fang, Y., Li, J., Michalski, G., and Zhang, L.: Triple oxygen
837   isotopic evidence for atmospheric nitrate and its application in source identification for
838   river systems in the Qinghai-Tibetan Plateau, The Science of the total environment, 688,
839   270-280, 10.1016/j.scitotenv.2019.06.204, 2019.

840   Xu, R., Hu, H., Tian, F., Li, C., and Khan, M. Y. A.: Projected climate change impacts on future
841   streamflow of the Yarlung Tsangpo-Brahmaputra River, Global and Planetary Change, 175,
842   144-159, 10.1016/j.gloplacha.2019.01.012, 2019.

843   Yang, K. and He, J.: China meteorological forcing dataset (1979–2018), National Tibetan
844   Plateau   Data   Center   [data   set],
845   https://doi.org/10.11888/AtmosphericPhysics.tpe.249369.file, 2019.

846   Yao, T., Masson-Delmotte, V., Gao, J., Yu, W., Yang, X., Risi, C., Sturm, C., Werner, M., Zhao,
847   H., He, Y., Ren, W., Tian, L., Shi, C., and Hou, S.: A review of climatic controls on δ18O
848   in precipitation over the Tibetan Plateau: Observations and simulations, Reviews of
849   Geophysics, 51, 525-548, 10.1002/rog.20023, 2013.

850   Yde, J. C., Knudsen, N. T., Steffensen, J. P., Carrivick, J. L., Hasholt, B., Ingeman-Nielsen, T.,
851   Kronborg, C., Larsen, N. K., Mernild, S. H., Oerter, H., Roberts, D. H., and Russell, A. J.:
852   Stable oxygen isotope variability in two contrasting glacier river catchments in Greenland,
853   Hydrology and Earth System Sciences, 20, 1197-1210, 10.5194/hess-20-1197-2016, 2016.

854   Yong, B., Wang, C.-Y., Chen, J., Chen, J., Barry, D. A., Wang, T., and Li, L.: Missing water
855   from the Qiangtang Basin on the Tibetan Plateau, Geology, 49, 867-872, 10.1130/g48561.1,
856   2021.

857   Yoshimura, K., Kanamitsu, M., Noone, D., and Oki, T.: Historical isotope simulation using
858   Reanalysis   atmospheric   data,   Journal   of   Geophysical   Research,   113,
859   10.1029/2008jd010074, 2008.

860   Zhang, F., Zhang, H. B., Hagen, S. C., Ye, M., Wang, D. B., Gui, D. W., Zeng, C., Tian, L. D.,
861   and Liu, J. S.: Snow cover and runoff modelling in a high mountain catchment with scarce
862   data: effects of temperature and precipitation parameters, Hydrol. Process., 29, 52–65,
863   https://doi.org/10.1002/hyp.10125, 2015.

864   Zhang, Z., Chen, X., Cheng, Q., and Soulsby, C.: Storage dynamics, hydrological connectivity
865   and flux ages in a karst catchment: conceptual modelling using stable isotopes, Hydrology

866   and Earth System Sciences, 23, 51-71, 10.5194/hess-23-51-2019, 2019.

867

868 **List of Tables**

869

870 **Table 1.** Summary of precipitation and stream water samples in the YTR and KR catchments.

Catchment (Station)	Year	Sampling dates (weekly)	Precipitation sample number	Stream sample number
YTR (Nuxia)		14/Mar to 23/Oct	86	34
YTR (Yangcun)	2005	17/Mar to 05/ Oct	59	30
YTR (Nugesha)		14/Mar to 22/ Oct	45	25
YTR (Lazi)		06/ Jun to 22/Sep	42	22
	2006	04/Jun to 11/Nov	24	31
	2007	23/Apr to 09/ Oct	39	25
KR (Wengguo)	2010	05/May to 18/ Oct	63	23
	2011	28/Mar to 06/Nov	69	32
	2012	16/ Jun to 22/ Sep	42	14

871
872

Table 2. Calibrated parameters of the THREW-T model

Symbol	Unit	Physical descriptions	Value range
nt	-	Manning roughness coefficient for hillslope	0-0.2
WM	cm	Tension water storage capacity, used in Xinanjiang model to calculate saturation area	0-10
B	-	Shape coefficient used in Xinanjiang model to calculate saturation area	0-1
KKA	-	Coefficient to calculate subsurface runoff in $Rg=KKD \cdot S \cdot K^S_S \cdot (y_S/Z)^{KKA}$, where S is the topographic slope, K^S_S is the saturated hydraulic conductivity, y_s is the depth of saturated groundwater, Z is the total soil depth	0-6
KKD	-	See description for KKA	0-0.5
T_0	°C	Temperature threshold above which snow and glacier melt	-5-5
DDF_N	mm/°C/day	Degree day factor for snowmelt	0-10
DDF_G	mm/°C/day	Degree day factor for glacier melt	0-10
$C1$	-	Coefficient to calculate the runoff concentration process using Muskingum method: $O_2=C_1 \cdot I_1+C_2 \cdot I_2+C_3 \cdot O_1+C_4 \cdot Q_{lat}$, where I_1 and O_1 is the inflow and outflow at prior step, I_2 and O_2 is the inflow and outflow at current step, Q_{lat} is lateral flow of the river channel, $C_3=1-C_1-C_2$, $C_4=C_1+C_2$	0-1
$C2$	-	See description for $C1$	0-1

Table 3. Descriptions of water sampling scenarios in the three numerical experiments. $\delta^{18}O_{GM}$ is the assumed glacier meltwater isotope signature and $\overline{\delta^{18}O_{PR}}$ refers to the long term mean isotope signature of precipitation.

Experiment	Scenarios	Isotope data conditions
Benchmark model running in the YTR basin	BM_YTR	Using assumed glacier meltwater isotope as: $\delta^{18}O_{GM}=\overline{\delta^{18}O_{PR}}$ - 5‰ Using IsoGSM outputs that were corrected by sample measurements of precipitation isotope from four sampling sites Using all available stream water samples in the study period to calibrate the model
Benchmark model running in the KR catchment	BM_KR	Using all available stream water samples in the study period to calibrate the model
Experiment 1: Estimate of glacier meltwater isotope	G_Δ1	Assuming glacier meltwater isotope as: $\delta^{18}O_{GM}=\overline{\delta^{18}O_{PR}}$ - 1‰
	G_Δ3	Assuming glacier meltwater isotope as: $\delta^{18}O_{GM}=\overline{\delta^{18}O_{PR}}$ - 3‰
	G_Δ7	Assuming glacier meltwater isotope as: $\delta^{18}O_{GM}=\overline{\delta^{18}O_{PR}}$ - 7‰
	G_Δ9	Assuming glacier meltwater isotope as: $\delta^{18}O_{GM}=\overline{\delta^{18}O_{PR}}$ - 9‰
Experiment 2: Site sampling data of precipitation isotope	P_1station	Using IsoGSM outputs corrected by measurements of precipitation isotope collected at one station (Nuxia) in YTR
	P_2stationNY	Using IsoGSM outputs corrected by measurements of precipitation isotope collected at two stations (Nuxia and Yangcun) in YTR
	P_2stationNL	Using IsoGSM outputs corrected by measurements of precipitation isotope collected at two stations (Nuxia and Lazi) in YTR
Experiment 3: Stream water sampling strategy for model evaluation	RT_YTR_BM	Sampling strategy: time series sampling; Sampling timing: wet season; Sampling frequency: weekly; Duration of sampling period: 1 year: Number of sampling site: 1 station
	RT_YTR_WholeYear	Same to RT_YTR_BM, but with the sampling timing as the whole study years
	RT_YTR_Monthly	Same to RT_YTR_BM, but with the sampling frequency as monthly
	RT_YTR_2year	Same to RT_YTR_BM, but with the duration of sampling period as only 2 years
	RT_YTR_3year	Same to RT_YTR_BM, but with the duration of sampling period as only 3 years
	RT_YTR_2station	Same to RT_YTR_BM, but with the number of sampling site as 2 stations
	RT_YTR_4station	Same to RT_YTR_BM, but with the number of sampling site as 4 stations
	RS_YTR_Main	Sampling strategy: spatially distributed sampling in a single field campaign; Location of sampling site: along the main stream
	RS_YTR_Tributary	Same to RS_YTR_Main, but using stream water samples from additional sites along the tributaries
	RT_KR_1year	Sampling strategy: time series sampling; Duration of sampling period: 1 year
	RT_KR_2year	Same to RT_KR_1year, but with the duration of sampling period as 2 years
	RT_KR_3year	Same to RT_KR_1year, but with the duration of sampling period as 3 years
	RT_KR_4year	Same to RT_KR_1year, but with the duration of sampling period as 4 years
	RT_KR_5year	Same to RT_KR_1year, but with the duration of sampling period as 5 years

Table 4. Contributions (%) of runoff components in the YTR basin and KR catchment estimated by different calibration variants in the benchmark scenario.

Runoff Component	YTR basin		KR catchment	
	Bi-objective calibration*	Tri-objective calibration	Bi-objective calibration	Tri-objective calibration
Rainfall	62.8 (±6.5)	70.7 (±2.5)	46.4 (±5.0)	43.9 (±1.4)
Snowmelt	10.8 (±1.1)	12.2 (±0.4)	22.6 (±2.4)	21.4 (±0.7)
Glacier melt	26.4 (±7.5)	17.1 (±2.9)	31.0 (±7.4)	34.6 (±2.0)
Surface runoff	52.1 (±10.5)	44.7 (±6.7)	62.0 (±10.9)	75.1 (±3.3)
Subsurface runoff	47.9 (±10.5)	55.3 (±6.7)	38.0 (±10.5)	24.9 (±3.3)

*: Values in brackets refer to the standard deviation of the contribution of runoff component produced by the behavioral parameter sets.

884 **Table 5**. Benchmark parameter set and corresponding model behavior that are used to produce
885 stream water $\delta^{18}O$ data for model calibration in experiment 3 in YTR basin.

Parameter value		Model behavior	
nt	0.09	NSE_{dis} (Nuxia,calibration)	0.87
WM	0.92	NSE_{dis} (Nuxia,validation)	0.80
B	0.62	$RMSE_{SCA}$ (calibration)	0.08
KKA	3.22	$RMSE_{SCA}$ (validation)	0.12
KKD	0.14	NSE_{iso}	0.58
T_0	1.59	NSE_{dis} (Yangcun)	0.85
DDF_N	8.04	NSE_{dis} (Nugesha)	0.76
DDF_G	8.28	Contribution of rainfall	70%
$C1$	0.0004	Contribution of snowmelt	12%
$C2$	0.075	Contribution of glacier melt	18%
		Contribution of baseflow	56%

886

List of Figures
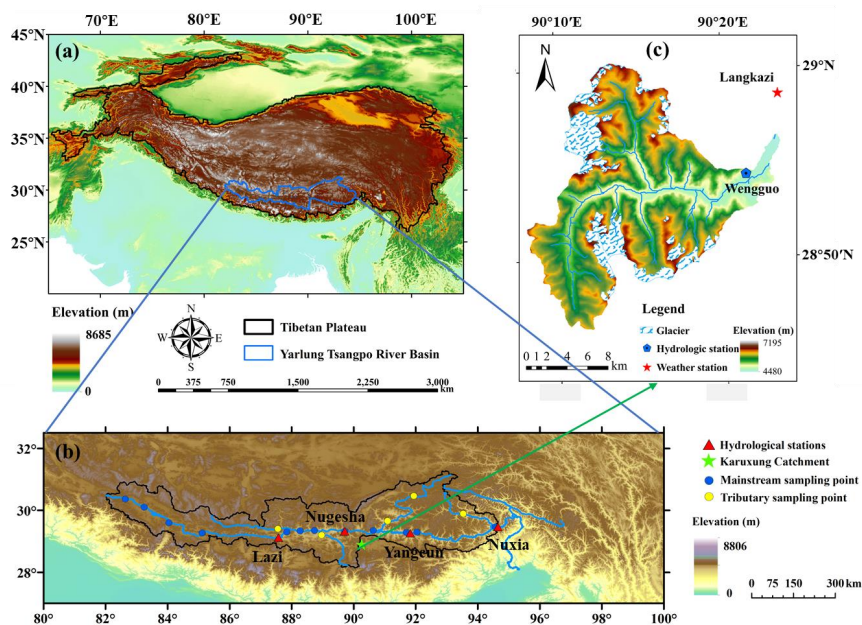
Figure 1. Locations and topography of the (a) Tibetan Plateau, (b) Yarlung Tsangpo river basin and (c) Karuxung catchment. Triangles in figure b refer to hydrometric stations and sampling sites for precipitation and stream water isotope. Dots in figure b refer to assumed stream water sampling locations in RD_YTR scenarios.

895
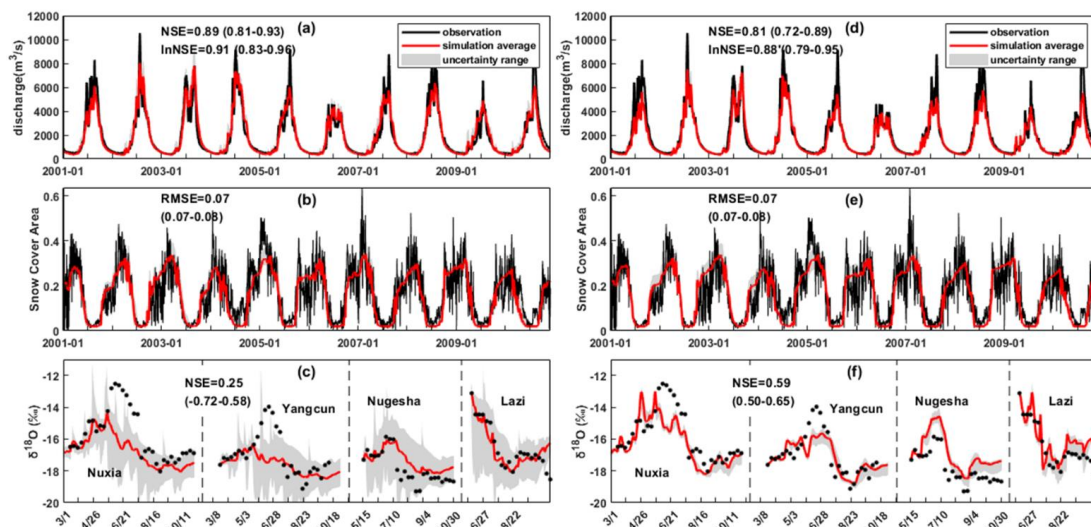
Figure 2. Uncertainty ranges and metrics values of the simulated discharge (Nuxia station),

SCA, and stream δ^{18}O (at four stations during 2005) in the YTR basin, that were produced by

the behavioral parameter sets of a bi-objective calibration (a-c) and a tri-objective (d-f)

calibration in the benchmark model running.

900

901
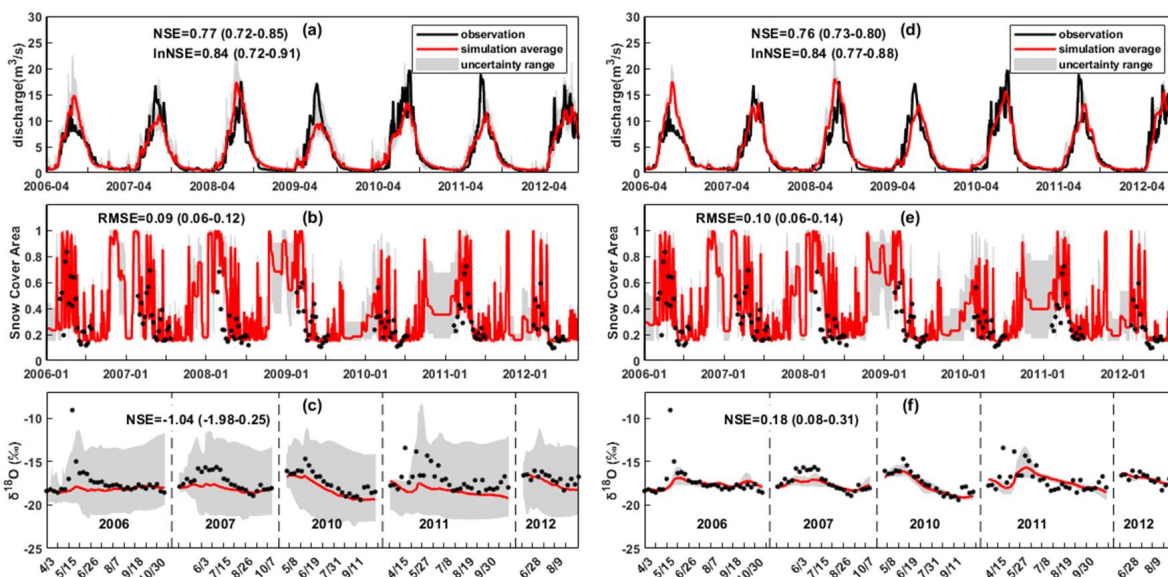
Figure 3. Uncertainty ranges and metrics values of the simulated discharge, SCA, and stream

$\delta^{18}O$ in the KR catchment produced by the behavioral parameter sets of a bi-objective

calibration (a-c) and a tri-objective (d-f) calibration in the benchmark model running.

905
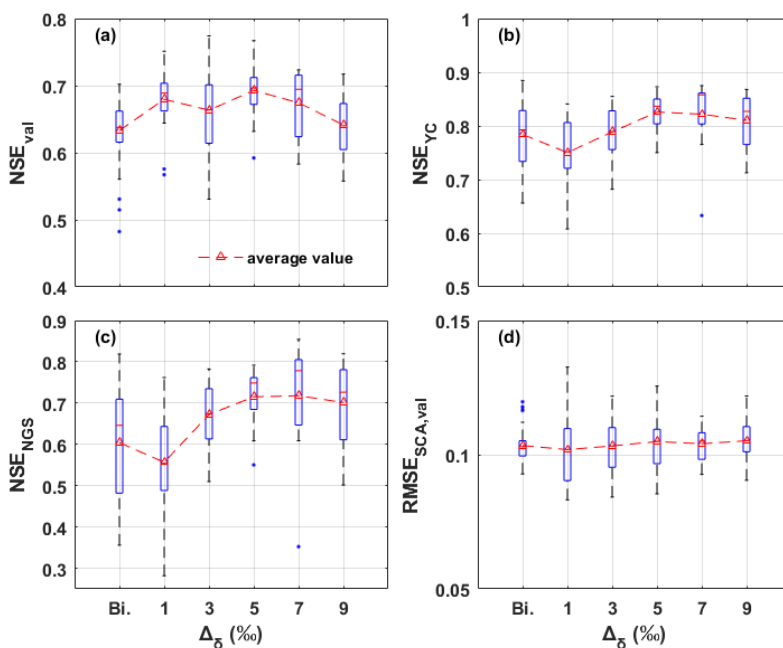
906
907 **Figure 4.** Model performances in simulating discharge and SCA in the YTR basin in validation
908 period/station produced by the behavioral parameter sets of scenarios using different glacier
909 meltwater isotope inputs (experiment 1). Subplot (a) and (d) are the performances for Nuxia
910 streamflow and SCA simulation in validation period, respectively. Subplot (b) and (c) are the
911 performances for streamflow simulation in internal stations Yangcun and Nugesha, respectively.
912
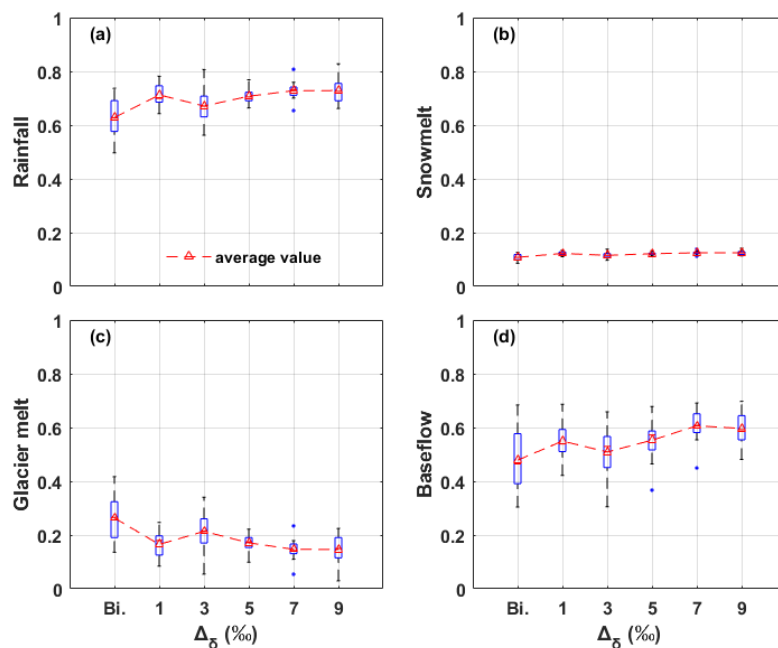
Figure 5. Runoff component contributions in the YTR basin estimated by the behavioral parameter sets of scenarios in experiment 1.

917
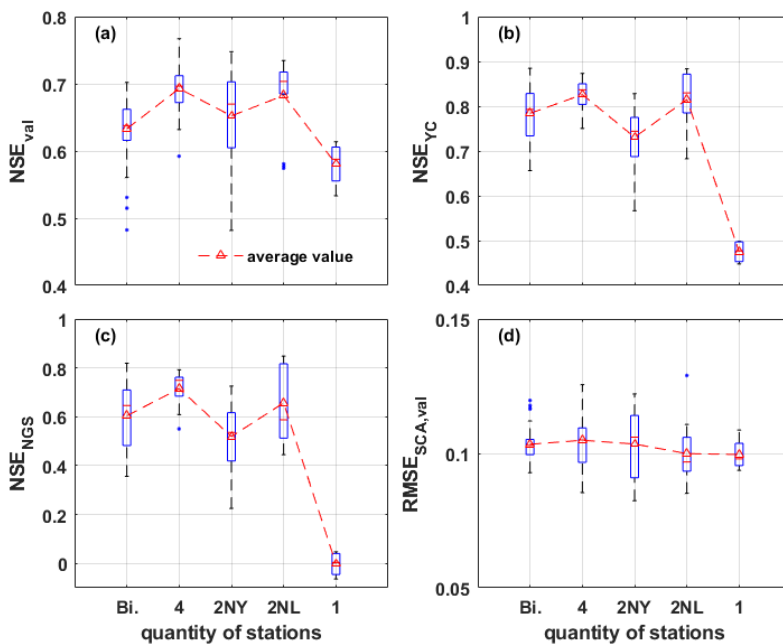
Figure 6. Model performances in simulating discharge and SCA validation period/station in YTR basin produced by the behavioral parameter sets of scenarios using precipitation isotope measurements from different sampling sites (experiment 2). Subplot (a) and (d) are the performances for Nuxia streamflow and SCA simulation in validation period, respectively. Subplot (b) and (c) are the performances for streamflow simulation in internal stations Yangcun and Nugesha, respectively.

924

925
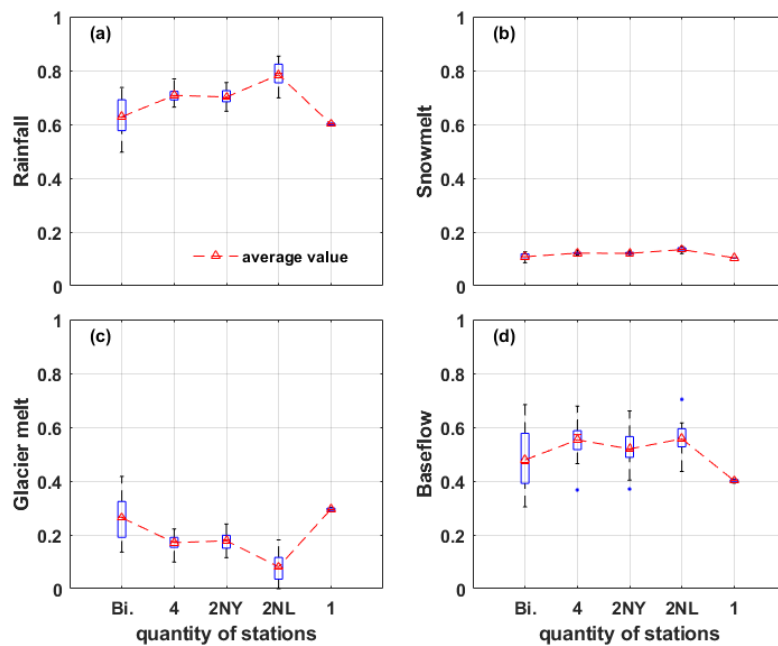
Figure 7. Runoff component contributions in the YTR basin estimated by the behavioral

parameter sets of scenarios in experiment 2.

928

929
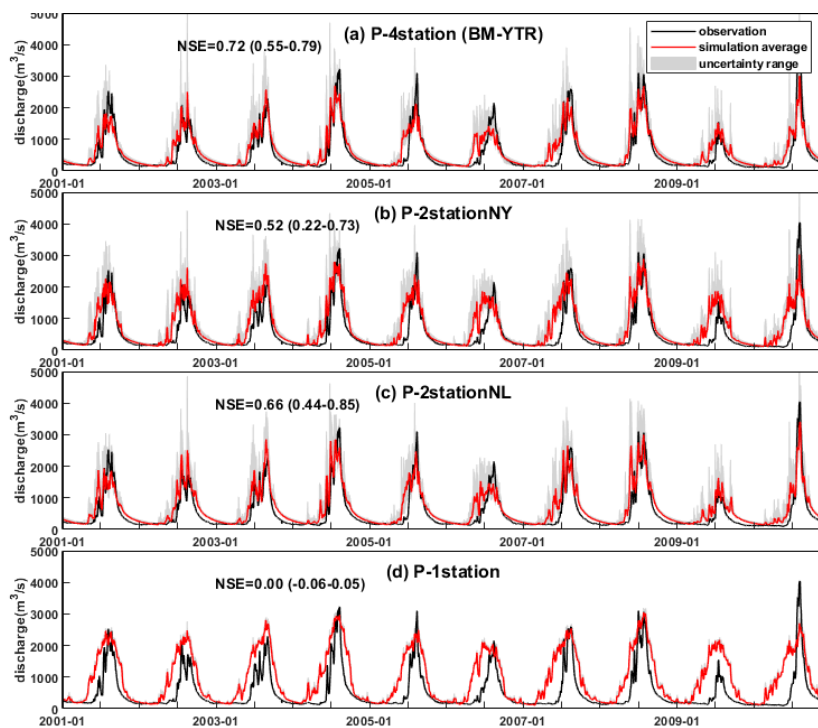
Figure 8. Uncertainty range and metrics values of simulated discharge at Nugesha station

produced by the behavioral parameter sets of each scenario in experiment 2.

932
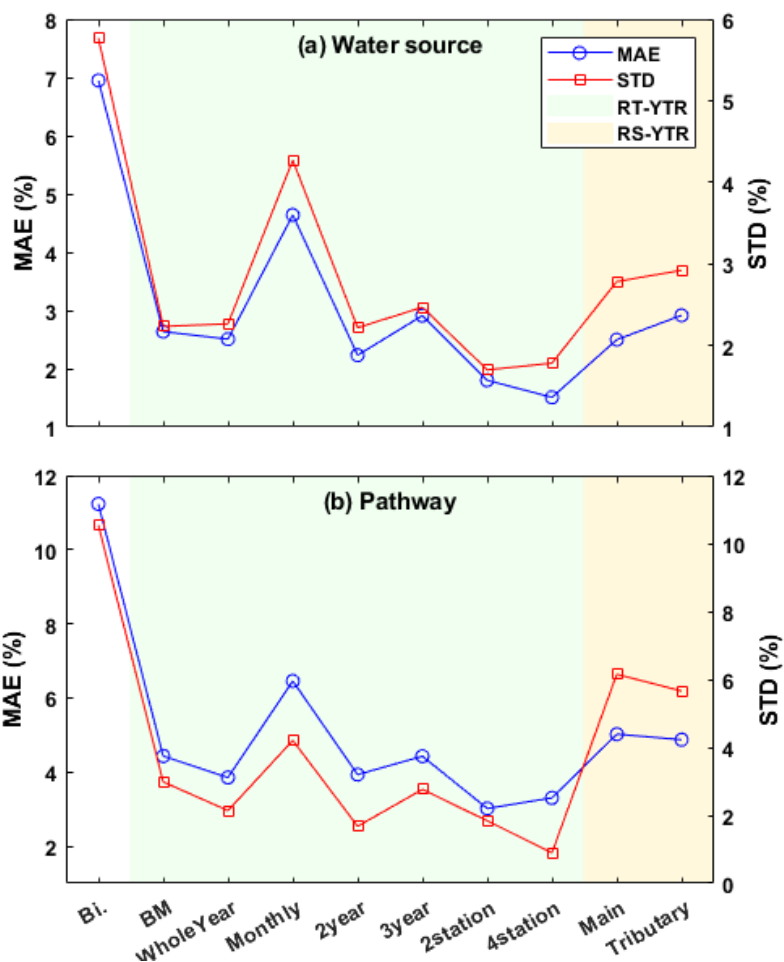
Figure 9. Accuracy and uncertainty metrics of estimated CRCs in the YTR basin derived from the different stream water sampling strategies (experiment 3). (a) for CRCs quantified under the definition of water source and (b) for CRCs quantified under the definition of runoff pathway.

939
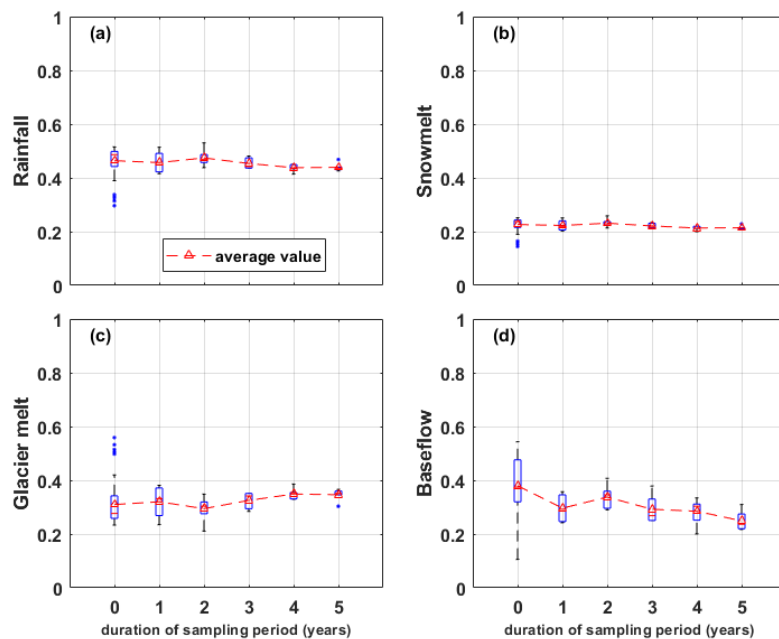
Figure 10. Uncertainties of the contributions of (a) rainfall, (b) snowmelt, (c) glacier melt and

941   (d) baseflow in the KR catchment, estimated by scenarios with different durations of

942   sampling period (experiment 3).

943
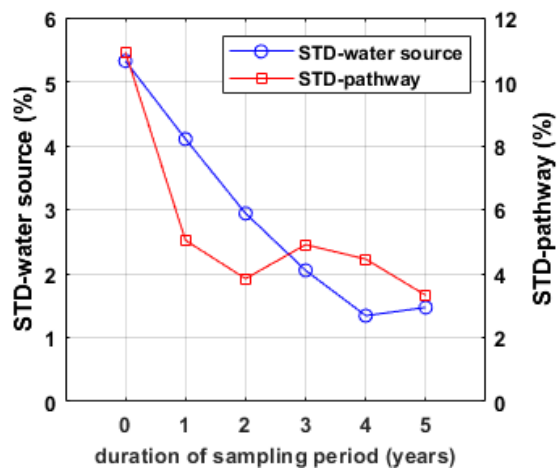
944

945 **Figure 11.** Uncertainty metrics of estimated CRCs in the KR catchment estimated by

946 scenarios with different durations of sampling period.

947